Available online at www.sciencedirect.com
ScienceDirect
Earth and Planetary Science Letters 257 (2007) 47–59
EPSL
www.elsevier.com/locate/epsl

Preservation of methane generated during serpentinization of upper mantle rocks: Evidence from fluid inclusions in the Nidar ophiolite, Indus Suture Zone, Ladakh (India)

Himanshu K. Sachan [a,*], Barun K. Mukherjee [a], Robert J. Bodnar [b]

[a] *Wadia Institute of Himalayan Geology, Dehra Dun-248001, India*
[b] *Department of Geosciences, Virginia Tech, Blacksburg, VA-24061, U.S.A.*

Received 22 December 2006; received in revised form 9 February 2007; accepted 9 February 2007
Available online 16 February 2007
Editor: R.W. Carlson

Abstract

The Nidar Ophiolite Complex (NOC) within the Indus Suture Zone in Eastern Ladakh, India, represents a suprasubduction zone (SSZ) ophiolite from a fore-arc setting. The lower part of the ophiolite sequence is comprised of ultramafic upper mantle rocks that are Mg-rich (Fo in olivine >90–92) and contain 2–7% Cr-spinel. Pure-methane (CH_4) fluid inclusions occur in olivine from partially serpentinized harzburgite and dunite from the NOC. Homogenization temperatures range from −160 °C to −108 °C, and freezing behavior combined with Raman analyses indicate that the inclusions contain no other gaseous species. The majority of the inclusions appear to be of secondary origin although some isolated inclusions of indeterminate origin were observed. CH_4 in the Nidar ophiolite was generated as a by-product of serpentinization of ultramafic rocks in the mantle wedge above the subducting slab, coupled with the complete consumption of water during hydration of serpentine. The presence of the lizardite polymorph of serpentine is consistent with formation in a rock-dominated system (low water activity) that was being deformed in a non-isotropic stress environment. The observed fluid inclusion isochores suggest various degrees of reequlibration during the history of the rocks, with the more extreme (high P) isochores most closely approximating the serpentinization conditions during prograde metamorphism at temperatures <600 °C and pressures in excess of about 2 kbars. These results support previous studies that have shown that early-formed fluid inclusions in mantle-derived rocks may be preserved during tectonic uplift to the surface and maintain the original mantle chemical signature.

Keywords: Nidar ophiolite; serpentinization; lizardite; antigorite; methane fluid inclusions; Raman spectroscopy

1. Introduction

Fluid inclusions in mantle xenoliths indicate that CO_2 is the dominant carbon-bearing fluid species in the upper mantle [1–5]. However, reduced carbon species are sometimes reported from primary mantle minerals, and some workers have suggested that the mantle may contain primordial methane (CH_4) and other hydrocarbons [6,7]. Other workers suggest that the deeper upper mantle may be more reduced than more shallow mantle environments [8–10], and that CH_4-bearing fluids may become oxidized to produce CO_2 as they migrate to shallower levels in the mantle.

* Corresponding author.
E-mail address: hksachan@wihg.res.in (H.K. Sachan).

0012-821X/$ - see front matter © 2007 Elsevier B.V. All rights reserved.
doi:10.1016/j.epsl.2007.02.023

While CO_2 is the dominant carbon-bearing species in fresh upper mantle samples, CH_4 and other reduced fluid species, including hydrogen, are commonly reported from upper mantle samples that have undergone serpentinization. Thus, CH_4 (and other hydrocarbons) in submarine hydrothermal vent fluids is thought to be generated during serpentinization of upper mantle peridotite by interaction with seawater in the subsurface [11–13]. Similarly, on the basis of He and H isotopes, Abrajano and coworkers [14] proposed a mantle origin for CH_4 gas seeps in the serpentinized Zambales ophiolite (Philippines). CH_4- and N_2-bearing fluid inclusions have also been reported from deformed Alpine-type ultramafic rocks [15], and other workers [16] interpret CH_4-bearing inclusions in eclogites to represent preserved pre-metamorphic fluids generated during serpentinization of peridotite in a subduction environment. In this paper, we describe CH_4 fluid inclusions

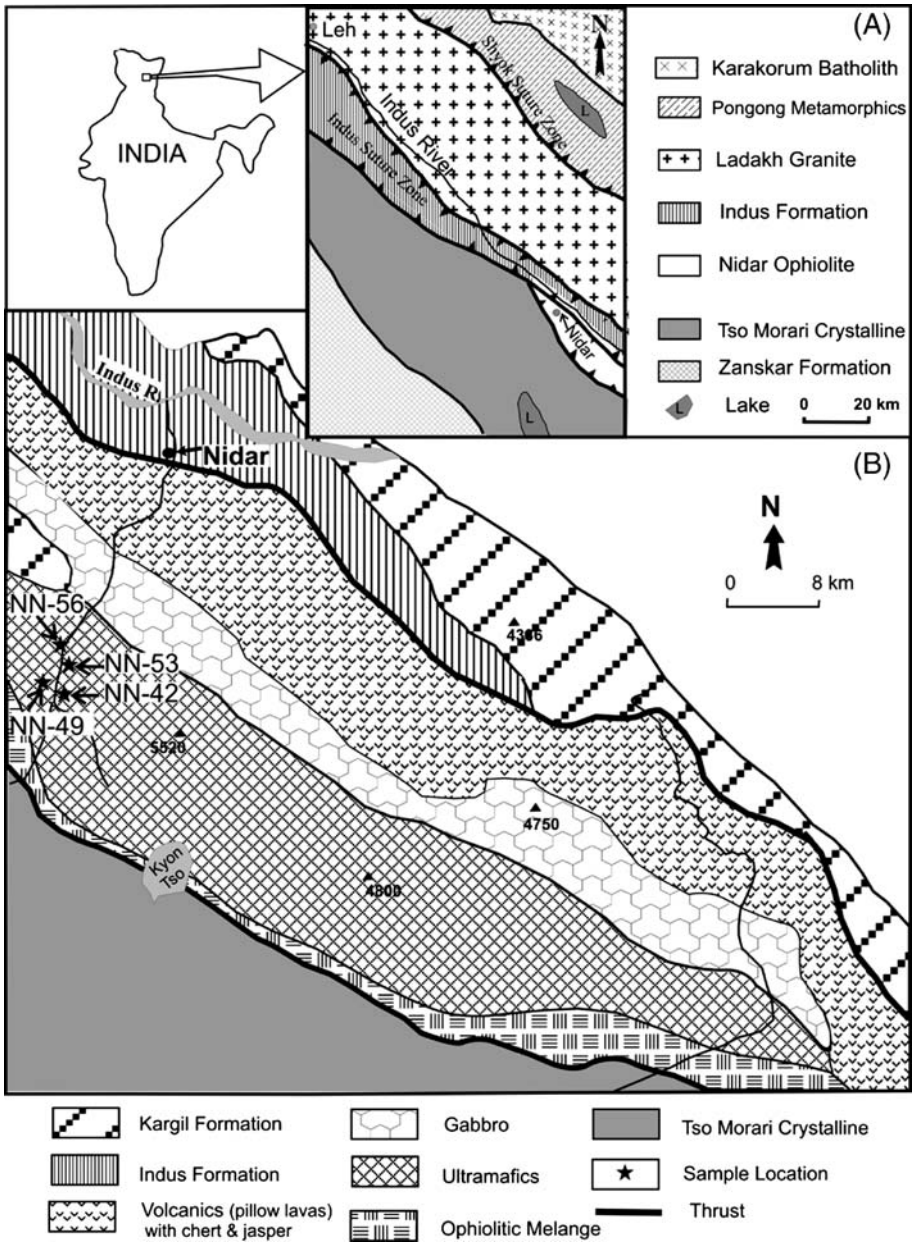

Fig. 1. Geological map of study area showing the location of the Nidar ophiolite (Inset) and sample locations (NN-42, NN-49, NN-53, NN-56) (Modified after [21]).

associated with serpentinized olivine in upper mantle rocks from the Nidar Ophiolitic Complex of the Indus Suture zone, Ladakh, India.

2. Geological setting

The Nidar Ophiolite Complex (NOC) is part of the Indus Suture Zone in Eastern Ladakh, India and represents a suprasubduction zone (SSZ) ophiolite from a fore-arc setting [17]. A Cretaceous age for the ophiolite has been inferred on the basis of fossils contained in the chert unit of the sequence [18]. The Nidar ophiolite was emplaced along the Indus Suture Zone during India–Asia continental collision and was associated with a steeply-dipping subduction zone [19]. The life cycle of SSZ ophiolites such as the Nidar ophiolite, from birth through death to resurrection (emplacement by obduction onto a passive margin or accretionary uplift during collision), is often geologically short [20].

The NOC has a north-dipping thrust contact with the metamorphic rocks of the Tso Morari crystalline complex to the south (Fig. 1). To the north, the NOC has a thrust contact (south dipping) with sedimentary units of the Indus Formation. The converging thrust contacts along

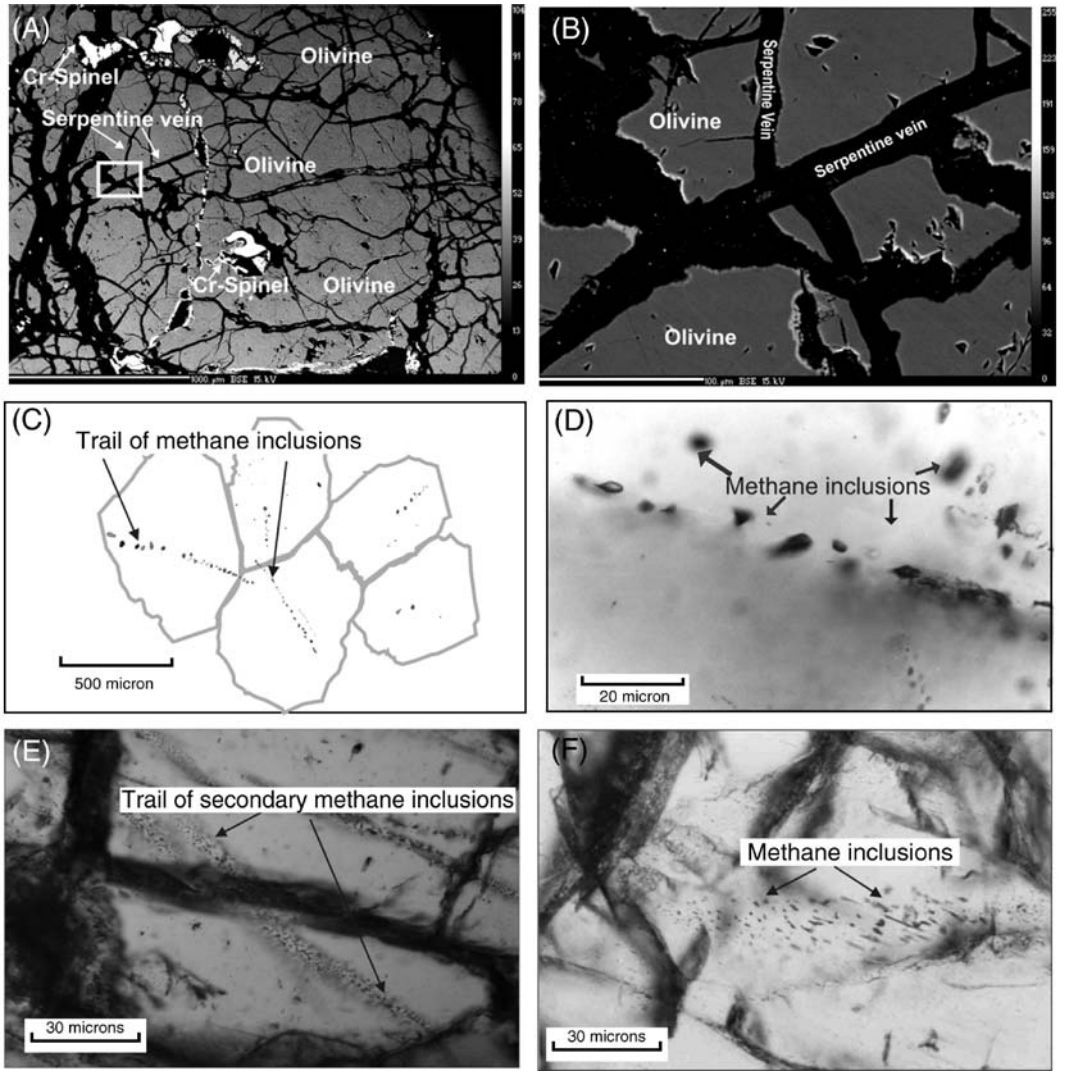

Fig. 2. (A) Backscatter electron image of chromite–harzburgite containing serpentine, olivine and Cr-spinel. (B) Backscatter electron image showing serpentine veins cutting olivine grains. (C) Sketch showing the occurrence of secondary methane inclusions along a trail in olivine. (D) Photomicrograph showing an intragrain trail as well as isolated methane inclusions. (E) Photomicrograph showing two intersecting intergrain trails that crosscut an olivine grain. (F) Intergrain trail of methane inclusions in olivine.

the southern and northern margins of the NOC suggest that it represents a root zone [21]. The southernmost unit of the NOC is the Zildat ophiolite melange that has experienced blueschist facies metamorphism [17]. Its northern margin has a thrust contact with the Nidar ophiolite. The Nidar ophiolite has a variable thickness (~3 to ~10 km) along its strike and is best developed in the Nidar–Kyun Tso section where it is ~8 km thick [22].

The Nidar ophiolite is composed of three mappable units, beginning with the lowermost ultramafic unit in the south, with gabbroic rocks in the middle, and andesitic–rhyolitic volcanics and volcanogenic sediments with chert as the uppermost unit in the north (Fig. 1). The ultramafic unit varies from chromite–harzburgite at the bottom to chromite–dunite at the top and shows a weak to moderate degree of serpentinization (≈10–20%; Fig. 2A). The chromite–harzburgite is widely distributed and is overthrust by Puga Gneisses of the Tso Morari crystalline complex. The chromite–dunite contains minor amounts of ortho- and clinopyroxenes. Chromite occurs as veins and as disseminated crystals in the chromite-dunite [23]. Minor pyroxenite veins, dominated by coarse-grained clinopyroxene and ranging from 1–10 cm wide, are observed in the ultramafics and overlying gabbros.

Both olivine gabbro and hornblende gabbro occur in a wide zone between the dunite and pillow lava sequence. Plagioclase, pyroxene (augite), olivine and hornblende are the main phases in both types. The gabbroic rocks vary from micro-gabbroic to coarse-grained rocks and lack compositional layering.

The overlying volcano-sedimentary unit includes basic to acidic volcanics. Basaltic-andesite flows predominate at lower stratigraphic levels and show poorly preserved pillow structures. The lower pillow lavas are intruded by dolerite dikes, whereas upper pillow lavas do not contain dikes and are subalkaline to rhyolitic in composition [24]. The upper volcanic unit grades into intercalated volcanic sediments with chert, jasperoid, shale, siltstone, volcanic sandstone, and conglomerate. The uppermost levels consist of acidic volcanics intercalated with pyroclastic deposits comprising ash flows, tuffs, lapillistone and volcanic breccias.

3. Mineralogy

Approximately 30 samples of dunite, harzburgite and chromite were collected from the lowermost ultramafic unit of the Nidar ophiolite (Fig. 1). The samples appear to be representative of the rocks present, based on color, degree of alteration and position within the sequence. After petrographic studies of all samples, representative samples were selected and analyzed by electron microprobe (Jeol-733 Superprobe) at IIT, Roorkee (India). The analytical conditions for spot analysis were 15 kV of accelerating potential and 15 nA sample current. Two samples each of chromite–dunite (NN–42, NN-49; Fig. 1) and chromite–harzburgite (NN-53 and NN-56; Fig. 1) were selected for detailed petrographic, mineralogical, microthermometric and Raman analysis. Serpentine mineral analyses and backscatter electron (BSE) images were obtained using a Cameca SX-100 electron microprobe at the Wadia Institute of Himalayan Geology, Dehra Dun, India. The operating conditions were 15 kV and 20 nA with a beam diameter of 1 μm. Natural mineral samples were used for calibration, except that synthetic oxides were used for Mn and Ti. A PAP correction was applied using software provided with the microprobe.

The studied samples are mostly coarse-grained. Olivine grains occur as small islands surrounded by serpentine, with individual grains ranging from <1 mm

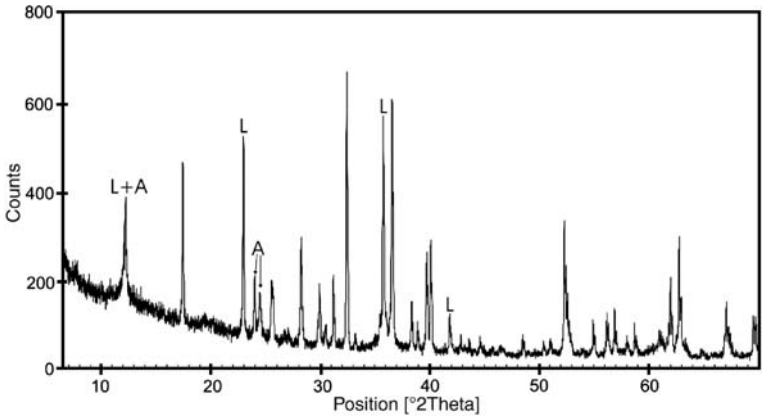

Fig. 3. XRD pattern of serpentine vein material from sample NN-53 obtained using Cu_{K_α} excitation.

to ~2 mm (Fig. 2 A and B). The olivine grains are sometimes elongated. The ortho- and clinopyroxene grains are ≤2 mm. Clinopyroxene is often associated with interstitial brown spinel that exhibits vermicular shape. Some euhedral spinels are associated with olivine. Serpentine group minerals lizardite and antigorite occur as veins that crosscut olivine grains, dividing them into numerous optically-continuous smaller islands (Fig. 2 A and B). The textural relationships and abundance of serpentine minerals are consistent with other ophiolites that have undergone low degrees of serpentinization under water-limited conditions [25]. Lizardite and antigorite in the Nidar samples were identified based on XRD (Fig. 3). Textures and habits of lizardite and antigorite revealed by SEM analysis (Fig. 4) are consistent with the occurrence of these minerals in other weakly to moderately serpentinized ultramafic rocks [25]. Thus, lizardite appears as plates or laths (Fig. 4A, C), compared to the more elongated and columnar appearance of antigorite (Fig. 4 B). Most veins contain both lizardite and antigorite. However, later serpentine veins that crosscut and in some cases offset earlier serpentine veins appear to contain relatively more antigorite, compared to the earlier veins. This observation is consistent with the inferred P–T evolution of these rocks as described in Section 5.3, P–T conditions of serpentinization.

The mineral chemistry of the samples studied has been presented previously [17], and only a summary is provided here (Table 1). The chromite–harzburgite consists of 56–89% Mg-rich olivine (Fo>90), 13–37% orthopyroxene, 1–10% clinopyroxene, and ~7% Cr-spinel. The chromite–dunite is composed mostly of Mg-rich olivine (Fo>92) and contains about 7% clinopyroxene, 2–4% spinel and rare orthopyroxene. Orthopyroxene and clinopyroxene are Mg-rich, with X_{Mg}= 0.91–0.92 and 0.92–0.95, respectively. The clinopyroxenes are diopsidic in composition. The Na_2O and TiO_2 concentrations are very low in clinopyroxene and the Al_2O_3 content (1.38–2.11%) is similar to oceanic mantle rocks. Spinels are Cr-rich (>60 wt.% Cr_2O_3) but have low TiO_2 (≤0.01 wt.%). The high Mg# of minerals in the studied rocks combined with the low TiO_2 content in spinel and clinopyroxene is consistent with crystallization from primitive (tholeiitic) or andesitic (boninitic) magma.

Compositions of lizardite and antigorite are shown in Table 2. Lizardite contains 1.24–2.22 wt.% Al_2O_3 and 2.18–3.05 wt.% FeO, compared to 3.42–3.64 wt.% and 4.04–5.03 wt.%, respectively, in antigorite. The elevated Al_2O_3 and FeO in antigorite is consistent with compositions reported for this mineral in other serpentinized ophiolites [26].

4. Fluid Inclusions

4.1. Petrography

Fluid inclusions were studied in doubly polished wafers ranging from about 120 to 150 μm thick. Characteristics of the fluid inclusions, including their distribution pattern, shape, size and phase relationships were defined using standard procedures for inclusions in metamorphic rocks [27,28].

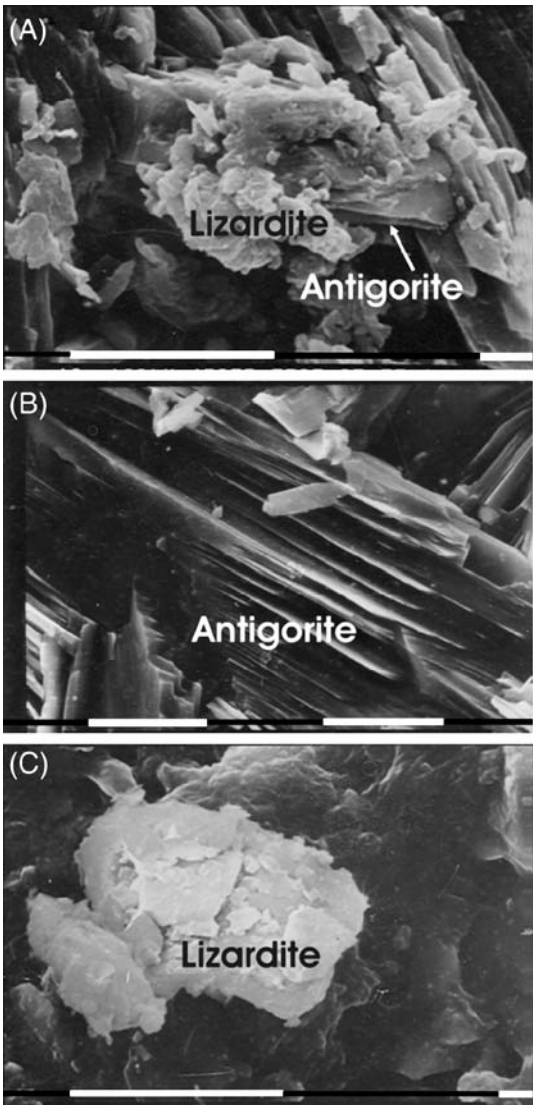

Fig. 4. SEM images of antigorite and lizardite in sample NN-53 from the Nidar ophiolite ultramafic unit. Scale bar represents 10 μm in all images. (A). Platy lizardite and elongated antigorite crystals (B) Antigorite, showing columnar pattern and elongation in one direction. (C) Lizardite, occurring in sheets of semicircular plates.

Table 1
Representative chemical composition of olivine, orthopyroxene, Cr-spinel and clinopyroxene in Nidar ophiolite samples

Sample	NN 42	NN 49	NN 53	NN 56	NN 42	NN 49	NN 53	NN 56	NN 42	NN 49	NN 53	NN 56	NN 42	NN 49	NN 53	NN 56
	Olivine				Orthopyroxene				Cr-Spinel				Clinopyroxene			
SiO_2	41.69	41.5	42.04	41.45	58.56	57.78	56.1	57.86	–	–	–	–	53.91	59.28	54.78	53.68
Al_2O_3	0.01	0.01	0.01	0.01	1.48	1.31	1.38	2.11	10.65	10.69	10.66	10.24	2.18	2.16	2.16	2.13
FeO	7.61	7.24	7.94	8.12	5.53	5.49	5.37	5.63	28.22	25.12	28.68	27.34	2.29	2.26	2.2	2.19
MgO	50.32	49.87	50.23	50.93	33.68	34.18	34.58	32.76	9.61	9.4	10.84	8.28	16.34	15.98	16.21	15.34
MnO	0.67	1.21	0.16	0.17	0.14	0.13	0.1	0.09	0.52	0.64	0.52	0.76	0.07	0.06	0.06	0.08
CaO	0.04	0.04	0.01	0.02	0.38	0.49	1.1	0.91	–	–	–	–	24.27	24.82	24.08	24.39
TiO_2	–	–	–	–	–	0.01	0.01	0	0.04	–	0.02	0.2	0.06	0.05	0.04	0.07
Na_2O	–	–	–	–	0.08	0.07	0.06	0.06	–	–	–	–	0.07	0.08	0.07	0.07
Cr_2O_3	–	0.08	0.03	0.04	0.48	0.46	0.45	0.46	50.01	53.26	50.08	52.81	0.1	0.12	0.09	0.2
NiO	0.32	0.41	0.41	0.94	–	–	–	–	–	–	–	–	–	–	–	–
ZnO	–	–	–	–	–	–	–	–	0.22	0.14	0.14	0.11	–	–	–	–
Total	100.66	100.36	100.83	99.02	100.33	99.92	99.15	99.92	99.28	99.28	100.93	99.55	99.29	99.75	99.71	99.03
Cations																
Si	1.007	1.007	1.012	0.998	1.99	1.97	1.923	1.97	–	–	–	–	1.96	2.03	1.985	1.98
Al	0.00	0.00	0.00	–	0.059	0.058	0.055	0.084	0.415	0.418	0.405	0.403	0.093	0.087	0.092	0.092
Fe	0.154	0.149	0.16	0.137	0.157	0.157	0.132	0.16	0.781	0.697	0.774	0.763	0.069	0.064	0.066	0.067
Mg	1.811	1.803	1.803	1.843	0.928	0.949	0.881	0.758	0.474	0.465	0.522	0.412	0.889	0.816	0.875	0.844
Mn	0.014	0.025	0.003	–	0.004	0.003	0.002	0.002	0.014	0.017	0.014	0.021	0.002	0.001	0.001	0.002
Ca	0.001	0.001	–	0.004	0.013	0.018	0.04	0.033	–	–	–	–	0.094	0.911	0.935	0.965
Na	–	–	–	–	0.005	0.004	0.003	0.003	–	–	–	–	0.004	0.005	0.004	0.004
Cr	0.00	0.00	0.002	0.001	0.012	0.012	0.012	0.012	1.308	1.397	1.279	1.39	0.002	0.003	0.002	0.003
Ni	0.006	0.006	0.012	0.019	–	–	–	–	–	–	–	–	–	–	–	–
Ti	–	–	–	–	–	–	–	–	0.00	–	–	–	0.001	0.001	0.001	0.001
Forsterite (%)	92.2	92.5	91.8	93.1	–	–	–	–	–	–	–	–	–	–	–	–
Mg#	–	–	–	–	91.55	91.97	91.99	91.19	48.85	52.07	51.37	44.47	92.7	92.6	92.9	92.5
Cr#	–	–	–	–	–	–	–	–	75.91	76.97	76.02	77.56	–	–	–	–

Note: NN-42 and NN-49=Chromite–dunite; NN-53 and NN-56=Chromite–harzburgite.
Oxide concentrations in weight percent; Cations are per formula unit Mg#=atomic [Mg/(Mg+Fe)]×100; Cr#=atomic [Cr/(Cr+Al)]×100.

Olivine contains numerous single-phase fluid inclusions along healed fracture planes that crosscut grain boundaries and pass into adjacent grains (Fig. 2C, D, E and F). These planar arrays represent secondary inclusions [2] or intergrain trails [28]. Rare 15–20 μm fluid inclusions appear to be isolated (Fig. 2C) but none of them can be considered unambiguously primary.

4.2. Microthermometry

Microthermometric measurements were conducted on a Linkam THSM 600 stage at Virginia Tech and at the Wadia Institute. Fifty-two inclusions in chromite–harzburgite and 39 inclusions in chromite–dunite were measured. On cooling, the single-phase inclusions solidified below −190 °C. All the inclusions showed initial melting around −182 °C, which is the triple point of pure CH_4 [29], suggesting that the inclusions do not contain any other gas species such as N_2. No solid phases (e.g., CO_2) other than CH_4 were observed.

Inclusions in chromite–harzburgite homogenize to the liquid phase at −160 to −112 °C (Fig. 5A). Inclusions in

Table 2
Representative chemical compositions of serpentine minerals in the studied samples based on EPMA analysis

Sample No.	NN-42	NN-49	NN-53	NN-42	NN-49	NN-53
	Lizardite			Antigorite		
SiO_2	40.76	39.29	40.98	41.9	41.22	41.27
AI_2O^3	2.22	1.87	1.24	3.44	3.42	3.64
Cr_2O_3	0:29	0.36	0.28	0.4	0.58	0.49
MgO	40.88	39.6	39.2	37.98	37.52	37.69
FeO*	2.18	2.81	3.05	4.04	5.03	4.95
MnO	0.05	0.05	0.03	0.12	0.09	0.11
NiO	0.18	0.18	0.17	0.18	0.23	0.21
TOTAL	86.56	84.16	84.95	88.06	88.09	88.3
Cations						
Si	1.918	1.911	1.969	1.947	1.929	1.924
Al	0.123	0.107	0.07	0.188	0.188	0.2
Fe	0.085	0.114	0.122	0.157	0.196	0.193
Cr	0.01	0.013	0.01	0.014	0.021	0.018
Mg	2.867	2.871	2.808	2.631	2.617	2.619
Mn	0.001	0.002	0.001	0.004	0.003	0.004
Ni	0.006	0.007	0.006	0.006	0.008	0.006

Note: NN-42 and NN-49 are dunites; NN-53 is a harzburgite.

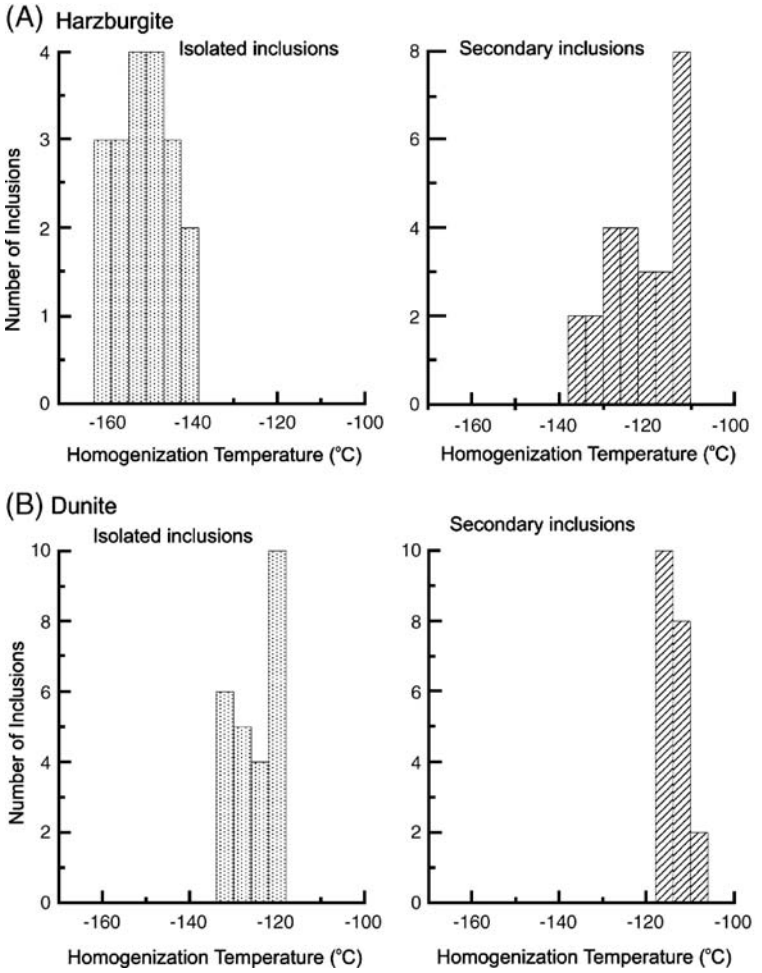

Fig. 5. Histogram of homogenization temperatures of CH_4 fluid inclusions in chromite–harzburgite (A) and in chromite–dunite (B).

chromite-dunite homogenize to the liquid phase at −132 to −108 °C (Fig. 5B). In both cases, isolated inclusions generally homogenize at lower temperatures than those along obvious fractures. The range in homogenization temperatures suggests (see Section 5.2, Preservation of fluid inclusions) that the inclusions may have reequilibrated volumetrically by some unknown amount [30].

4.3. Raman Analysis

Several inclusions, representing the range in measured homogenization temperatures from the harzburgite and the dunite, were analyzed at room temperature with a DILOR-XY Raman microprobe at Virginia Tech. The analytical conditions were as follows: Laser excitation, 514 nm; laser power, 100 mw; analysis time, 128 s. Analyses were conducted using a 100X microscope objective. The Raman peak positions were determined with an accuracy of ±2 cm^{-1}. A typical Raman spectrum of a CH_4 inclusion is shown in Fig. 6. The CH_4 peak occurs at about 2915 cm^{-1} and suggests internal pressures in the inclusions of a few hundred bars at room temperature [31]. No other gas species were detected in the fluid inclusions, consistent with the observed melting temperature of the inclusions and lack of solid phases other than CH_4 during cooling. Based on these observations, we conclude that the inclusions are pure CH_4.

5. Discussion

5.1. Origin of the CH_4

Any inferred origin for the CH_4 inclusions in the Nidar ophiolite must be consistent with textural, mineralogical and geochemical observations, including:

1. Serpentine veins contain both lizardite and antigorite (Fig. 4A, C)

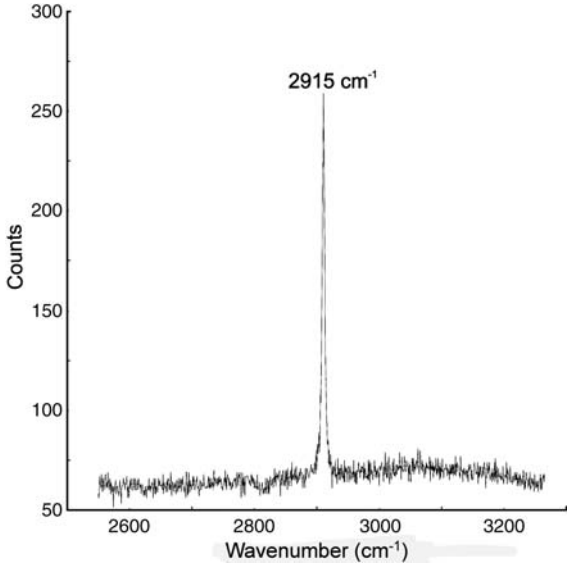

Fig. 6. Raman spectrum of a CH_4 fluid inclusion showing the characteristic ν_1 symmetric stretching band for CH_4.

2. Brucite ($Mg(OH)_2$) is not observed in the samples
3. CH_4 inclusions do not contain CO_2, H_2 or other gases
4. Aqueous inclusions are not observed in association with the CH_4 inclusions

Four possible sources of CH_4 have been identified for crustal and upper mantle rocks [32,33]. These include biological production, thermal cracking of higher hydrocarbons, outgassing of juvenile CH_4 and inorganic (Fisher–Tropsch) synthesis. The Nidar ophiolite contains chert sediments of submarine origin and, while a biological origin and breakdown of higher hydrocarbons as sources of CH_4 in the Nidar ophiolite cannot be ruled out, other sources appear to be more likely, as described below.

Most of the inclusions observed in Nidar samples occur along fractures that cut multiple grains and are clearly secondary in origin and were trapped at some time after the original rock-forming minerals formed; rare isolated inclusions of indeterminate origin were also observed. If these latter inclusions were primary, then they would have been trapped in the magma chamber when the host olivine formed. The CH_4 could have been sourced from the underlying fertile and non-degassed mantle [8–10]. However, this origin is inconsistent with magma sources in the suprasubduction zone environment where the ultramafic rocks were generated. Thus, an origin of the CH_4 in the primary mantle magma is considered to be an unlikely source.

During the past few decades it has become increasingly obvious that CH_4-rich fluids are associated with serpentinization of ultramafic rocks. Serpentinization of peridotite in the submarine and subduction zone environments can occur over a wide range of temperatures, from relatively low temperatures (100–200 °C) where the minerals chrysotile and lizardite ($Mg_3Si_2O_5(OH)_4$) are stable, and continuing to the upper stability limit of antigorite [$Mg_{48}Si_{34}O_{85}(OH)_{62}$] at about 620 °C [34,35]. CH_4-rich hydrothermal fluids have been observed venting along the Mid-Atlantic Ridge (MAR) in areas where serpentinized bodies occur on the seafloor [36,37], CH_4- and C_2H_6-rich pore waters were sampled during ODP Leg 125 at a serpentinized seamount in the Mariana forearc [38,39], and CH_4-bearing fluid inclusions occur in gabbroic rocks from ODP Hole 735B on the Southwest Indian Ridge [40]. CH_4 and H_2 have also been observed emanating from serpentinized bodies in the Zambales ophiolite in the Philippines [14]. More recently, CH_4- and H_2-rich fluids were discovered at the Lost City Hydrothermal Field that is located 15 km away from the spreading axis of the MAR [13] in an area where active serpentinization is occurring. Production of CH_4 during serpentinization in the sub-seafloor is now a widely recognized and accepted process, and it has been estimated that globally plutonic layer 3 in the oceanic crust contains 10^{19} g of abiogenic CH_4 generated by serpentinization of mafic and ultramafic rocks [41].

Observations listed above are consistent with serpentinization of the Nidar ophiolite by a process involving alteration of the fayalite component of olivine by a fluid containing water and carbon dioxide according to:

$$6Fe_2SiO_4 + 2H_2O + CO_2 = 4Fe_3O_4 + 6SiO_2(aq) + CH_4 \quad (1)$$

The CO_2 may be produced by magmatic degassing of an underlying magma body or, alternatively, could be released from CO_2 inclusions in olivine (as has been observed in some mantle xenoliths [5]) during the serpentinization process. Some workers [14] have also suggested that the source of carbon to produce CH_4 during serpentinization may be dissolved carbonate from calcareous sedimentary rocks that have been subducted and metamorphosed along with the igneous rocks.

Aqueous silica released by reaction (1) interacts with the forsterite component of the olivine to produce the serpentine mineral lizardite according to:

$$18Mg_2SiO_4 + 6SiO_2(aq) + 24H_2O = 12Mg_3Si_2O_5(OH)_4 \quad (2)$$

With increasing temperature lizardite becomes unstable and antigorite becomes the stable serpentine

phase. According to Evans [34], lizardite can be converted to antigorite in the presence of a silica-rich fluid according to:

$$16Mg_3Si_2O_5(OH)_4 + 2SiO_2(aq) = Mg_{48}Si_{34}O_{85}(OH)_{62} + H_2O \quad (3)$$

The serpentinization process in the Nidar ophiolite described by reactions (1)–(3) above is consistent with models which suggest that fluids in subduction zones are capable of transporting significant amounts of dissolved silica [42]. Note also that reactions (1) and (2) combined generate CH_4 but produce neither H_2 nor brucite. Additional support for the mechanism outlined above is that serpentinized peridotites containing brucite also contain aqueous fluid inclusions with up to 1 mol% H_2 (and no CH_4), and CH_4 inclusions are absent [43].

As noted earlier, most of the CH_4-bearing inclusions observed in the Nidar ophiolite occur along intergrain fractures and are interpreted to have formed during the serpentinization process. Importantly, the fluid inclusions did not reequilibrate compositionally during deformation and exhumation (although the inclusions probably did reequilibrate volumetrically, as described in Section 5.2). Hydrogen was not detected in the inclusions during Raman analysis, and this is consistent with reactions (1)–(3) in which hydrogen is not a product. Even if hydrogen were generated during serpentinization of the Nidar ophiolite and trapped in the inclusions, it is well known that hydrogen can move easily into or out of fluid inclusions at elevated temperature if they are subjected to gradients in oxygen (or hydrogen) fugacity [44–46]. During exhumation, the Nidar ophiolite would have been subjected to increasingly more oxidizing conditions as they approached the surface, generating an oxygen fugacity gradient between the inclusions and surrounding rock. This, in turn, would promote the diffusion of hydrogen out of the inclusions to produce pure CH_4 inclusions. Similar CH_4-bearing fluid inclusions produced during serpentinization and preserved during exhumation and deformation have been observed in eclogites [16].

The Zambales ophiolite in the Philippines is a suprasubduction zone ophiolite that formed in proximity to an island arc and is now located in a forearc setting [47]. The Zambales ophiolite is undergoing active serpentinization and may represent a modern analog of the Nidar ophiolite before its emplacement and exhumation [14]. Interestingly, the Zambales Ophiolite is known for its active CH_4 and H_2 gas seeps (Los Fuegos Eternos) that ignite to produce yellow-orange flames [48]. Based on chemical and stable and radiogenic isotopic analyses [14], the gases are interpreted to have been generated by reduction of H_2O and carbon (most likely from CO_2) during serpentinization. It is worth noting that the Zambales ophiolites are only partially serpentinized. Because it is much easier to maintain the low f_{O2} conditions required to generate CH_4 during serpentinization in a rock-dominated (H_2O-limited) system [14], we propose that the limited serpentinization observed in the Nidar ophiolites reflects a low water/rock ratio during serpentinization. This interpretation is in agreement with the presence of lizardite (rather than chrysotile) in the assemblage, as chrysotile seems to require fluid-filled pore space, whereas lizardite does not [34]. According to this scenario, all H_2O in the system was incorporated into serpentine and other hydrous minerals, consistent with the absence of aqueous fluid inclusions associated with the CH_4 inclusions.

5.2. Preservation of fluid inclusions

According to our interpretation, CH_4 inclusions in the Nidar ophiolite were trapped during serpentinization, most likely before emplacement and exhumation of the ophiolite. This requires that the inclusions were preserved as the ophiolite underwent emplacement and exhumation. During this process, the fluid inclusions may have been exposed to significantly different P–T conditions than those at which the inclusions formed.

The conditions that lead to reequilibration of fluid inclusions in nature are reasonably well understood [30,49–53], and techniques for recognizing fluid inclusions that have reequilibrated are well-established [51,52,54–56]. Inclusions in the Nidar ophiolite appear to have reequilibrated volumetrically without changing the fluid composition, as evidenced by variable homogenization temperatures (densities) of inclusions along an individual fracture [30]. Other examples of CH_4-bearing inclusions that have been preserved during metamorphism and deformation include those in the Isua Archean Greenstone belt (West Greenland), which are presumed to represent preserved remnants of fluids associated with serpentinization on the seafloor [57]. While the inclusions have reequilibrated to higher density during metamorphism, they have retained their original composition. Similarly, CH_4-bearing inclusions are preserved in the 375 Ma Lizard ophiolite (United Kingdom) that was metamorphosed at amphibolite-facies conditions [58], and CH_4-bearing inclusions from the Carpathian Mountains, Ukraine, show textural and microthermometric evidence of volumetric reequilibration without changing the fluid composition [52,56].

The exact P–T history experienced by the Nidar ophiolite is unknown (Section 5.3), although workers have inferred that serpentinization of other ophiolites (Zildat

ophiolite) in the Indus Suture Zone occurred at P–T conditions similar to those that produced nearby eclogites, with estimates ranging from 600 °C and 20 kbar [59] to 800 °C and 39 kbar [60]. We suggest that the Nidar ophiolite represents a pericollisional ophiolite [20] in which there is no significant time gap between the time of formation and its obduction onto the passive continental margin. As such, the Nidar ophiolite did not experience the extreme P–T conditions associated with other ophiolites in the region, as evidenced by the relatively low-grade metamorphic mineral assemblage and the limited extent of serpentinization observed in the Nidar samples.

5.3. P–T conditions of serpentinization

The P–T conditions of serpentinization can vary significantly, depending on the chemical composition of the original protolith and alteration mineralogy [34,35]. Several ophiolite assemblages have been identified within the Indus Suture Zone and, based on field observations and descriptions of the extent of alteration and the alteration mineralogy, it is clear that the P–T conditions of alteration (metamorphism) within this zone varied widely. For example, thermochronological studies of basalt samples from an ophiolitic melange of the Indus Suture Zone indicate that the rocks experienced post-collisional thermal activity at >500 °C [61]. Some workers report that gabbros in the Nidar ophiolite are highly metamorphosed in the amphibolite and greenschist facies with very few magmatic minerals preserved [62], and that serpentinization of the Nidar ophiolite and eclogitization within the Tso Morari unit both took place under similar conditions of 600 °C and 20 kbar [59]. [We note that the Nidar ophiolite samples in the study of Guillot et al. [59] have been incorrectly identified and actually come from the Zildat ophiolitic melange [17] that has undergone blueschist facies metamorphism]. Other workers report that the Nidar ophiolite and the Zildat Ophiolitic Melange are nearly undeformed and underwent only low grade metamorphism [63]. These widely varying estimates of the degree of alteration and the P–T conditions experienced by ophiolites in the Indus Suture Zone likely reflects a combination of assigning outcrops to incorrect units and the complicated geology of the region which juxtaposes rocks with very different P–T histories adjacent to one another.

The CH_4 inclusions in the Nidar ophiolite can be used to place constraints on the P–T history of the rocks. Isochores for the CH_4-bearing inclusions were estimated with the aid of the "FLINCOR" program [64]. Isochores for the isolated inclusions in chromite–harzburgite and chromite–dunite indicate a higher pressure of formation compared to inclusions that occur along fractures (Fig. 7), reflecting the greater tendency for fracture-hosted inclusions to reequilibrate, compared to isolated inclusions in the cores of mineral grains [30].

All serpentine veins in the Nidar ophiolite contain both lizardite and antigorite. However, veins that are clearly late (based on crosscutting relationships) appear to contain relatively less lizardite than earlier veins. This suggests that serpentinization took place during a prograde (heating) event with lizardite forming early (lower temperature) and antigorite forming later (higher temperature), and that the mineral phases were preserved during exhumation. The P–T stability ranges for these serpentine minerals in the $MgO–SiO_2–H_2O$ (MSH) system [34] are shown along with the fluid inclusion isochores on Fig. 7. The area of overlap of the fluid inclusion isochores with the stability ranges for lizardite and antigorite define a P–T region that extends from <100 °C and <2 kbars to about 600 °C and about 3–8 kbars. The upper end of this temperature range is consistent with temperatures of 400–600 °C predicted for the corner of the mantle wedge where oceanic crust

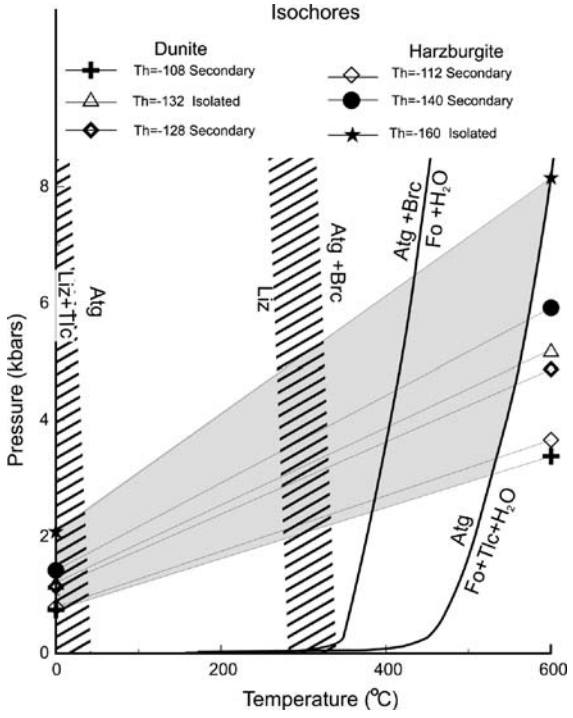

Fig. 7. P–T diagram showing isochores of CH_4 inclusions in chromite–harzburgite and dunite from the Nidar ophiolite sequence. Also shown are the stability fields of various minerals in the $MgO–SiO_2–H_2O$ (MSH) system [34]. Abbreviations: Liz = lizardite; Tlc = talc; Atg = antigorite; Brc = brucite; Fo = forsterite. The lined regions representing the Liz+Tlc=Atg and Atg+Brc=Liz reflect the uncertainty in the positions of these reactions.

meets forearc mantle above the subducting slab [37], and where the serpentinization is inferred to have occurred. Evans [34] reports that lizardite and antigorite may coexist at temperatures ≤300 °C, with only antigorite stable above this temperature, and this is consistent with textural relationships in the serpentine veins and with temperatures indicated by the CH_4 fluid inclusion isochores (Fig. 7).

If the fluid inclusion densities (homogenization temperatures) represent the original trapping conditions, then serpentinization must have also taken place somewhere within the broad temperature-pressure range shown on Fig. 7. However, the range in homogenization temperatures within an individual mineral grain and along an individual fracture suggests that the inclusions have either "stretched" or "contracted" in response to changing P–T conditions during emplacement and exhumation. The main effect of volumetric reequilibration of fluid inclusions is to shift the isochores to lower pressures (stretching) or higher pressures (contraction) for a given temperature, and examples of both processes have been documented in the literature [52,57]. Based on the tectonic environment, the Nidar ophiolite was probably emplaced and uplifted to the surface very rapidly [20,62] along an initially isothermal P–T path and this interpretation is consistent with the preservation of the serpentine mineral paragenesis described above. As such, the CH_4 fluid inclusions in the Nidar ophiolite would have reequilibrated by stretching to produce lower densities. In this case, the higher-pressure isochores shown on Fig. 7 would most closely approximate the original (prograde) formation conditions, whereas the lower pressure isochores would reflect conditions of exhumation. While the exact P–T path cannot be estimated from these data, it is clear that the P–T path followed by the Nidar ophiolite passed through the shaded region shown on Fig. 7 at some time during the serpentinization process.

6. Summary

The occurrence of CH_4 inclusions in the serpentinized Nidar ophiolite is consistent with laboratory results [11,65–67] and observations in modern submarine environments [13,36,38,68] where active serpentinization is occurring. During serpentinization, CO_2 was reduced to CH_4 that was then trapped along fractures in olivine. The lack of aqueous inclusions in association with the CH_4 inclusions is consistent with the presence of lizardite in the alteration assemblage. Lizardite (as opposed to chrysotile) forms by hydration of olivine and pyroxene in a rock dominated (low water activity) system at low supersaturation and lizardite is more likely to be preserved (compared to chrysotile) in a non-isotropically-stressed environment [34]. The hydration of olivine to produce lizardite is accompanied by volume expansion on the order of 40–50% [34]. This expansion serves to decrease permeability in the fractures where lizardite is forming, removing water through the hydration process and prohibiting other fluids from entering the fractures. Preservation of the CH_4 inclusions in the Nidar ophiolite is consistent with models for the life cycle of suprasubduction zone ophiolites (SSZ), which suggest that some serpentinized and buoyant SSZ ophiolites are obducted onto the passive margin shortly after formation and exhumed to the surface without being deeply buried. A final important conclusion of this study is that fluid inclusions in at least some altered, buried and exhumed mantle rocks retain the chemical signature of the deep crust and mantle, as others have previously suggested [16].

Acknowledgements

The first and second authors thank the Director of WIHG for permission to publish this work. The authors also thank Mr. Frank Harrison for assistance with Raman analyses. The authors are also grateful to Tom Andersen, Fons Van den Kerkhof, David Vanko and T. Tsunogae for comments on an earlier version of this manuscript. We especially thank Bernard Evans, whose review of this paper offered a clear and thorough summary of the geochemical implications (and limitations) of our observations, and led to a more rigorous and geochemically consistent interpretation of the data. Our interpretation of the environment required to generate CH_4 in the Nidar ophiolites was influenced significantly by comments provided by Bernard Evans in his review of this paper — we are grateful for his contribution and accept complete responsibility for any shortcomings that remain. NSF Grants EAR-952668 and EAR-0125918 provided partial funding for this research to RJB.

References

[1] E. Roedder, Liquid CO_2 inclusions in olivine-bearing nodules and phenocrysts from basalts, Am. Mineral. 50 (1965) 1746–1782.
[2] E. Roedder, Fluid Inclusions, Mineralogical Society of America, Washington, D.C., 1984, 644 pp.
[3] T. Andersen, W.L. Griffin, S.Y. O'Reilly, Primary sulphide and melt inclusions in mantle derived magacrysts and pyroxenites, Lithos 20 (1987) 279–294.
[4] J.D. Pasteris, Fluid inclusions in mantle xenoliths, in: P.H. Nixon (Ed.), Mantle Xenoliths, John Wiley & Sons, Chichester, 1987, pp. 691–707.

[5] C. Szabó, R.J. Bodnar, Changing ascent rates of magmas in the Nógrád-Gömör Volcanic Field, North Hungary/South Slovakia: evidence from CO_2 inclusions in mantle xenoliths, Petrology 4 (1996) 221–230.
[6] T. Gold, S. Soter, The deep-earth gas hypothesis, Sci. Am. 242 (1980) 154–170.
[7] A.A. Giardini, C.E. Melton, R.S. Mitchell, The nature of the upper 400 km of the earth and its potential as a source for non-biogenic petroleum, J. Pet. Geol. 5 (1982) 173–190.
[8] C. Ballhaus, B.R. Frost, The generation of oxidized CO_2-bearing basaltic melts from reduced CH_4-bearing upper mantle sources, Geochim. Cosmochim. Acta 58 (1994) 4931–4940.
[9] C. Ballhaus, Is the upper mantle metal-saturated? Earth Planet. Sci. Lett. 132 (1995) 75–86.
[10] S.K. Simakov, Redox state of eclogites and peridotites from sub-cratonic upper mantle and a connection with diamond genesis, Contrib. Mineral. Petrol. 151 (2006) 282–296.
[11] D.I. Foustoukos, W.E. Seyfried Jr., Hydrocarbons in hydrothermal vent fluids: the role of chromium-bearing catalysts, Science 304 (2004) 1002–1005.
[12] D.S. Kelley, G.L. Fruth-Green, Abiogenic methane in deep-seated mid-ocean ridge environments: Insights from stable isotope analyses, J. Geophys. Res. 104 (1999) 10439–10460.
[13] D.S. Kelley, et al., A serpentine-hosted ecosystem: the Lost City Hydrothermal Field, Science 307 (2005) 1428–1434.
[14] T.A. Abrajano, N.C. Sturchio, J.K. Bohlke, G.L. Lyon, R.J. Poreda, C.M. Stevens, Methane-hydrogen gas seeps, Zambales ophiolite, Philippines: deep or shallow origin, Chem. Geol. 71 (1988) 211–222.
[15] A.L. Goncharnko, V.A. Simonov, Fluid inclusions in plastically deformed olivines from alpine-type ultramafics, Dokl. Akad. Sci. USSR Earth Sci. 276 (1986) 108–111.
[16] B. Fu, J.L.R. Touret, Y.-F. Zheng, Remnants of premetamorphic fluid and oxygen isotopic signatures in eclogites and garnet clinopyroxenite from the Dabie-Sulu terranes, eastern China, J. Metamorph. Geol. 21 (2003) 561–578.
[17] H.K. Sachan, Supra subduction zone origin of Nidar ophiolitic sequence, Indus Suture Zone, Ladakh: evidence from mineral chemistry of upper mantle rocks, Ofioliti 26 (2001) 23–32.
[18] N.S. Virdi, Indus-Tsangpo suture in the Himalaya: a crustal expression of the palaeo-subduction zone, Ann. Soc. Geol. Pol. 56 (1986) 3–31.
[19] M.L. Leech, S. Singh, A.K. Jain, S.L. Klemperer, R.M. Manickavasagam, The onset of India-Asia continental collision: early, steep subduction required by timing of UHP metamorphism in the western Himalaya, Earth Planet. Sci. Lett. 234 (2005) 83–97.
[20] J.W. Shervais, Birth, death and resurrection: the life cycle of suprasubduction zone ophiolites, Geochem. Geophys. Geosyst. 2 (2001).
[21] V.C. Thakur, D.K. Mishra, Tectonic framework of the Indus and Shyok suture zone in eastern Ladakh, northwest Himalaya, Tectonophysics 101 (1984) 207–220.
[22] V.C. Thakur, M.I. Bhat, Interpretation of tectonic environment of Nidar ophiolite: a geochemical approach, in: V.C. Thakur, K.K. Sharma (Eds.), Geology of the IndusSuture Zone, Wadia Institute of Himalayan Geology, Dehra Dun, 1983, pp. 21–31.
[23] H.K. Sachan, B.K. Mukherjee, Genesis of chromite in ophiolites from Indus Suture Zone, Ladakh India: evidence from mineral chemistry of solid inclusions in chromite, Himal. Geol. 24 (2003) 63–74.
[24] T. Ahmad, N.B.W. Harris, R. Islam, P.P. Khanna, H.K. Sachan, B.K. Mukherjee, Contrasting mafic magmatism in the Shyok and Indus Suture zone: geochemical constraints, Himal. Geol. 26 (2005) 34–40.
[25] H.M. Prichard, A petrographic study of the process of serpentinization in ophiolites and the ocean crust, Contrib. Mineral. Petrol. 68 (1979) 231–241.
[26] X.P. Li, M. Rahn, K. Bucher, Serpentinites of the Zermatt-Saas ophiolite complex and their textural evolution, J. Metamorph. Geol. 22 (2004) 159–177.
[27] J.L.R. Touret, Fluids in metamorphic rocks, Lithos 55 (2001) 1–26.
[28] A.M. Van den Kerkhoff, U.F. Hein, Fluid inclusion petrography, Lithos 55 (2001) 27–48.
[29] R.H. Goldstein, T.J. Reynolds, Systematics of fluid inclusions in diagenetic minerals, Soc. Sediment. Geol. Short Course 31 (1994) 199.
[30] R.J. Bodnar, Reequilibration of fluid inclusions, in: I. Samson, A. Anderson, D. Marshall (Eds.), Fluid Inclusions: Analysis and Interpretation, vol. 32, Mineralogical Association of Canada, 2003, pp. 213–230.
[31] J.C. Seitz, J.D. Pasteris, I.M. Chou, Raman spectroscopic characterization of mixtures-I quantitative composition and pressure determination of CH_4, N_2 and their mixtures, Am. J. Sci. 293 (1993) 297–321.
[32] M. Schoell, Multiple origins of methane in the Earth, Chem. Geol. 71 (1988) 1–10.
[33] J.A. Welham, Origin of methane in hydrothermal systems, Chem. Geol. 71 (1988) 183–198.
[34] B.W. Evans, The serpentine multisystem revisited: chrysotile is metastable, Int. Geol. Rev. 46 (2004) 479–506.
[35] B.W. Evans, W. Johannes, H. Oterdoom, V. Trommsdorff, Stability of chrysotile and antigorite in the serpentinite multisystem, Schweiz. Mineral. Petrogr. Mitt. 56 (1976) 79–93.
[36] J.L. Charlou, J.-P. Donval, Hydrothermal methane venting between 12°N and 26°N along the Mid-Atlantic Ridge, J. Geophys. Res. 98 (1993) 9625–9642.
[37] H. Bougault, J.-L. Charlou, Y. Fouquet, H.D. Needham, N. Vaslet, P. Appriou, P.J. Baptiste, P.A. Rona, L. Dmitried, S. Silanties, Fast- and slow-spreading ridges: structure and hydrothermal activity, ultramafic topographic highs, and CH_4 output, J. Geophys. Res. 98 (1993) 9643–9651.
[38] J.A. Haggerty, Fluid inclusion studies of chimneys associated with serpentinite seamounts in the Mariana forearc, in: R.J. Bodnar (Ed.), Second biennial Pan-American Conference on Research on Fluid Inclusions, vol. 2, Virginia Polytechnic Institute and State University, Blacksburg, VA U.S.A., 1989, p. 29.
[39] M.J. Mottl, J.A. Haggerty, Upwelling of Cl-poor, S and C-rich waters through a serpentinite seamount, Mariana Forearc, ODP Leg 125, American Geophysical Union, vol. 70, American Geophysical Union, San Francisco, 1989, p. 1382.
[40] D.A. Vanko, D.S. Stakes, Fluids in oceanic layer 3: evidence from veined rocks, Hole 735B, Southwest Indian Ridge, in: R.P.V. Herzen, R.P. Fox, A. Palmer, P.T. Robinson (Eds.), Proceedings of the Ocean Drilling Program, vol. 118, Ocean Drilling Program, College Station, TX, 1991, pp. 181–215.
[41] D.S. Kelley, G.L. Früh-Green, Abiogenic methane in deep-seated mid-ocean ridge environments: insights from stable isotope analyses, J. Geophys. Res. 104 (1999) 10439–10460.
[42] C.E. Manning, Effect of sediments on aqueous silica transport in subduction zones, in: D.W.S.G.E. Bebout, S.H. Kirby, J.P. Platt (Eds.), Subduction Top to Bottom, Geophysical Monograph Series, American Geophysical Union, Washington, D.C., 1996, pp. 277–284.

[43] A. Peretti, J. Dubessy, J. Mullis, B.R. Frost, Highly reducing condition during Alpine metamorphism of the Malenco peridotite (Sondrio, northern Italy) indicated by mineral paragenesis and H_2 in fluid inclusion, Contrib. Mineral. Petrol. 112 (1992) 329–340.
[44] J.A. Mavrogenes, R.J. Bodnar, Hydrogen movement into and out of fluid inclusions in quartz: Experimental evidence and geologic implications, Geochim. Cosmochim. Acta 58 (1994) 141–148.
[45] D.L. Hall, R.J. Bodnar, Methane in fluid inclusions from granulites: a product of hydrogen diffusion? Geochim. Cosmochim. Acta 54 (1990) 614–651.
[46] D.L. Hall, R.J. Bodnar, J.R. Craig, Evidence for postentrapment diffusion of hydrogen into peak metamorphic fluid inclusions from the massive sulfide deposits at Ducktown, Tennessee, Am. Mineral. 76 (1991) 1344–1355.
[47] K.M. Gillis, N.R. Banerjee, Hydrothermal alteration patterns in supra-subduction zone ophiolites, in: Y. Dilek, E.M. Moores, D. Elthon, A. Nicholas (Eds.), Ophiolites and Oceanic Crust: New Insights from Field Studies and the Ocean Drilling Program, Geological Society of America Special Paper, vol. 349, Geological Society of America, Boulder, CO, 2000, pp. 283–297.
[48] W.C. Stoll, Natural fires in South Lawis river valley, Zambales, P.I. Philipp. Geol. 7 (1959) 167–170.
[49] S.M. Sterner, R.J. Bodnar, Synthetic fluid inclusions. VII. Reequilibration of fluid inclusions in quartz during laboratory-simulated metamorphic uplift, J. Metamorph. Geol. 7 (1989) 243–260.
[50] M.O. Vityk, R.J. Bodnar, Do fluid inclusions in high grade metamorphic terranes preserve peak metamorphic density during retrograde decompression? Am. Mineral. 80 (1995) 641–644.
[51] M.O. Vityk, R.J. Bodnar, Textural evolution of synthetic fluid inclusions in quartz during re-equilibration, with applications to tectonic reconstruction, Contrib. Mineral. Petrol. 121 (1995) 309–323.
[52] M.O. Vityk, R.J. Bodnar, I.V. Dudok, Hydrocarbon inclusions in Marmarosh Diamonds: evidence for tectonic history of the folded Carpathians? Tectonophysics 255 (1996) 163–174.
[53] M.O. Vityk, R.J. Bodnar, C. Schmidt, Fluid inclusions as tectonothermobarometers: relation between P–T history and re-equilibration morphology during crustal thickening, Geology 22 (1994) 731–734.
[54] M.O. Vityk, R.J. Bodnar, Statistical microthermometry of synthetic fluid inclusions in quartz during decompression, Contrib. Mineral. Petrol. 132 (1998) 149–162.
[55] M.O. Vityk, R.J. Bodnar, J.-C. Doukhan, Synthetic fluid inclusions: XV. TEM investigation of plastic flow associated with re-equilibration of synthetic fluid inclusions in natural quartz, Contrib. Mineral. Petrol. 139 (2000) 285–297.
[56] M.O. Vityk, R.J. Bodnar, I. Dudok, Natural and synthetic re-equilibration textures of fluid inclusions in quartz (Marmarosh Diamonds): evidence for refilling under conditions of compressive loading, Eur. J. Mineral. 7 (1995) 1071–1087.
[57] J.R.L. Touret, Remnants of early Archean hydrothermal methane and brines in pillow-breccia from the Isua Greenstone Belt, West Greenland, Precambrian Res. 126 (2003) 219–233.
[58] L. Hopkinson, S. Roberts, Fluid evolution during tectonic exhumation of oceanic crust at a slow-spreading paleoridge axis: evidence from the Lizard ophiolite, U.K. Earth Planet. Sci. Lett. 141 (1996) 125–136.
[59] S. Guillot, K.H. Hattori, J. de Sogoyer, Mantle wedge serpentinization and exhumation of eclogites: insights from eastern Ladakh, northwest Himalaya, Geology 28 (2000) 199–2002.
[60] B.K. Mukherjee, H.K. Sachan, Y. Ogaswara, A. Muko, N. Yoshida, Carbonate-bearing UHPM rock from Tso-Morari region, Ladakh, India: possible petrological implications, Int. Geol. Rev. 45 (2003) 49–69.
[61] R. Bhutani, K. Pande, T.R. Venkatesan, Tectono-thermal evolution of the India–Asia collision zone based on ^{40}Ar–^{39}Ar thermochronology in Ladakh, India, Proc. Indian Acad. Sci. 113 (2004) 737–754.
[62] G. Maheo, H. Bertrand, S. Guillot, I.M. Villa, F. Keller, P. Capiez, The South Ladakh ophiolites (NW Himalaya, India): an intra-oceanic tholeiitic arc origin with implication for the closure of the Neo–Tethys, Chem. Geol. 203 (2003) 273–303.
[63] M. Schlup, A. Carter, M. Cosca, A. Steck, Exhumation history of eastern Ladakh revealed by $^{40}Ar/^{39}Ar$ and fission track ages: the Indus River—Tso Morari transect, NW Himalaya, J. Geol. Soc. (Lond.) 160 (2003) 385–399.
[64] P.E. Brown, FLINCOR: a microcomputer program for the reduction and investigation of fluid inclusion data, Am. Mineral. 74 (1989) 1390–1393.
[65] M.E. Berndt, D.E. Allen, W.E. Seyfried Jr., Reduction of CO_2 during serpentinization of olivine at 300 °C and 500 bar, Geology 24 (1996) 351–354.
[66] J. Horita, M.E. Berndt, Abiogenic methane formation and isotopic fractionation under hydrothermal conditions, Science 285 (1999) 1055–1057.
[67] T.M. McCollom, J.S. Seewald, A reassessment of the potential for reduction of dissolved CO_2 to hydrocarbons during serpentinization of olivine, Geochim. Cosmochim. Acta 65 (2001) 3769–3778.
[68] J.L. Charlou, J.P. Donval, E. Douville, P. Jean-Baptiste, J. Radford-Knoery, Y. Fouquet, A. Dapoigny, M. Stievenard, Compared geochemical signatures and the evolution of MenezGwen (37°50′N) and Lucky Strike (37°17N) hydrothermal fluids, south of the Azores Triple Junction on the Mid-Atlantic Ridge, Chem. Geol. 171 (2000) 49–75.